

Mott electrons in an artificial graphenelike crystal of rare earth nickelate

S. Middey,^{1,*} D. Meyers,¹ D. Doennig,² M. Kareev,¹ X. Liu,¹ Y. Cao,¹ Zhenzhong Yang,³ Jinan Shi,³ Lin Gu,^{3,4} P. J. Ryan,⁵ R. Pentcheva,^{2,6} J. W. Freeland,⁵ and J. Chakhalian¹

¹Department of Physics, University of Arkansas, Fayetteville, Arkansas 72701, USA

²Department of Earth and Environmental Sciences and Center of Nanoscience, University of Munich, D-80333 Germany

³Beijing National Laboratory for Condensed-Matter Physics and Institute of Physics, Chinese Academy of Sciences, Beijing 100190, P. R. China

⁴Collaborative Innovation Center of Quantum Matter, Beijing 100190, Peoples Republic of China

⁵Advanced Photon Source, Argonne National Laboratory, Argonne, Illinois 60439, USA

⁶Department of Physics, University of Duisburg-Essen, Duisburg, D-47057 Germany

Deterministic control over the periodic geometrical arrangement of the constituent atoms is the backbone of the material properties, that along with the interactions define the electronic and magnetic ground state. Following this notion, a bilayer of a prototypical rare-earth nickelate, NdNiO₃, combined with a dielectric spacer, LaAlO₃, has been layered along the pseudo cubic [111] direction. The resulting artificial graphenelike Mott crystal with magnetic 3d electrons has antiferromagnetic correlations. In addition, a combination of resonant X-ray linear dichroism measurements and *ab-initio* calculations reveal the presence of an ordered orbital pattern, which is unattainable in either bulk nickelates or nickelate based heterostructures grown along the [001] direction. These findings highlight another promising venue towards designing new quantum many-body states by virtue of geometrical engineering.

The intense research activities over the last several decades on transition metal oxides (TMO) have demonstrated the successful manipulation of various correlated electron phenomena including the metal-insulator transition, high temperature superconductivity, magnetism, colossal magnetoresistance, multiferroicity, etc. by chemical doping and various external stimuli [1–3]. The continuous advancements in ultra-thin film growth techniques with atomic precision provide additional opportunities for further control through epitaxial constraint, quantum confinement and heterostructuring with dissimilar layers [4–8]. To date, the vast majority of the reported work has been focused on systems grown along the pseudo-cubic [001] direction. The idea that a geometrical motif of an underlying lattice can also be a very powerful tool for generating new quantum many-body states has been vividly highlighted by the discoveries of exotic electronic and topological phases in geometrically frustrated materials (e.g. spin liquid, spin ice, magnetic monopole, etc.) [9–12]. Following this paradigm, very recently several theoretical proposals have been put forward to utilize a few unit cells of a TMO heterostructured along the pseudo-cubic [111] directions [13–23]. This geometrically engineered motif relies on the presence of an artificially buckled honeycomb (i.e. graphenelike) [14–16] (see Fig. 1), dice lattices [13] for bilayers, trilayers of ABO₃ perovskites respectively and alternating triangular and Kagome atomic planes in A₂B₂O₇ pyrochlore lattices [20]. In spite of these exciting opportunities, to-date the experimental works on (111)-oriented thin films have been very limited [24–30] due to the extreme challenge of stabilizing materials along the strongly polar [111] direction [31].

Towards the realization of this idea, we have explored heterostructures based on the rare-earth nickelate NdNiO₃. Over the past few years, following the prediction of high T_c cuprate-like physics in LaNiO₃/LaAlO₃ heterostructures [32, 33], a number of artificial quantum structures with rare earth nickelate

RENiO₃ ($RE = \text{La...Eu}$ etc.), grown along the pseudo-cubic (001) direction have been extensively investigated [34–45]. In the bulk, RE nickelates exhibit a multitude of interesting electronic phases including the metal-insulator transition (MIT), paramagnetic metallic and insulating phases, and charge ordering with a strong dependence of the transition temperatures on the size of the rare-earth ion RE^{3+} [46]. Magnetically, these materials demonstrate an unusual E' -type antiferromagnetic ordering [47].

Due to the markedly different arrangements of atoms along

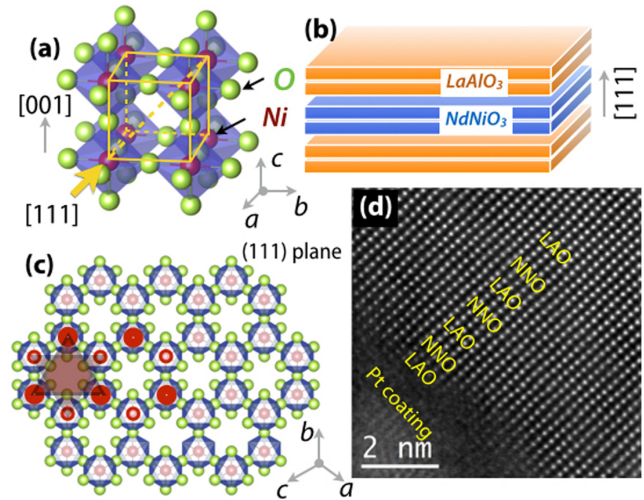


FIG. 1. (a) One unit cell of the perovskite structure. A RE ion, located at the center of the cube, has been omitted for clarity. (b) Bilayer of NdNiO₃ sandwiched between layers of dielectric LaAlO₃ along the pseudo cubic [111] direction. (c) Schematic of a (111) bilayer that forms a buckled honeycomb lattice. The Ni atoms on individual (111) plane are highlighted by thin and thick red circles respectively. (d) HAADF-STEM image of [2NdNiO₃/4LaAlO₃]_{x3} superlattice, grown on LaAlO₃ (111) substrate.

the [111] direction versus [001], the theoretical calculations [15–19] for (111) oriented bilayers of nickelates (Fig. 1(a)-(c)), predict the emergence of novel quantum many-body and interacting topological ground states, which are unattainable in both bulk nickelates and (001) grown heterojunctions. Intriguingly, in the weakly correlated limit the theory anticipates the emergence of several exotic topological phases (e.g. Dirac half-metal, quantum anomalous Hall effect, and ferromagnetic nematic phase) due to the buckled honeycomb lattice with d^7 electrons, even without spin-orbit coupling which is normally required to realize the topological states [48]. However, due to the confinement of electrons along the out of plane direction, effective electron-electron correlation is enhanced compared to the bulk Nickelates and the model Hamiltonian calculations in the strongly correlated limit predict that orbitally ordered states are the lowest energy phases as compared to the bulk-like charge ordered phase [16–18].

In this paper, we report on the electronic and magnetic properties of geometrically engineered [2 uc NdNiO₃/4 uc LaAlO₃] (2NNO/4LAO) superlattices (SL) grown epitaxially on LAO (111) substrates (uc = unit cell in pseudocubic setting). Synchrotron based X-ray resonant magnetic scattering (XRMS) measurements showed that these artificial graphene-like Mott crystals have antiferromagnetic correlations. In addition, the combination of resonant X-ray linear dichroism measurements and first-principles GGA+ U calculations reveal the presence of an orbitally ordered pattern, which has not been realized earlier in the rare-earth nickelates. The presence of this new orbitally polarized ground state is linked to the strong reduction in the hopping interaction in the buckled honeycomb lattice geometry combined with the breaking of local symmetry.

Epitaxial [2NNO/4LAO] \times 3 superlattices oriented along the [111] direction were grown by pulsed laser interval deposition [49]. In order to avoid the formation of any oxygen deficient phase due to the interfacial polar discontinuity [50], LaAlO₃ (111) substrates were used. The possibility of faceted surface has been excluded by the streaks in RHEED (reflection high energy electron diffraction) patterns recorded during the growth and after cooling the film to room temperature [51]. STEM (scanning transmission electron microscopy) experiments were performed using a spherical aberration-corrected JEM-ARM200F operated at 200 kV and high angle annular dark field (HAADF) imaging was performed using the collection semiangle of about 70-250 mrad. The observation of clear interfaces between NNO and LAO layers (Fig. 1(d) and also see supplemental [51]) further confirms the desired layer by layer growth of the superlattice. XRMS (x-ray resonant magnetic scattering) and XLD (x-ray linear dichroism) measurements were carried out at 4-ID-C beam line of Advanced Photon Source (APS) at Argonne National laboratory. X-ray diffraction measurements were carried out at 6-ID-B beam line of APS. DFT calculations were performed using the all-electron, full-potential linearized augmented plane wave (FP-LAPW) method, as implemented in the WIEN2k code [52, 53]. For the exchange-correlation potential we used

the generalized gradient approximation (GGA) [54], while the GGA+ U method [55] was used to take into account static local electronic correlations. All calculations were carried out using $U = 5$ eV, $J = 0.7$ eV (Ni 3d); $U = 8$ eV (Nd 4f). The lateral lattice constant was fixed to the LAO (111) substrate, while the out-of-plane lattice parameter was optimized. Octahedral tilts and distortions were fully considered.

In order to map the investigated SL into the theoretically proposed phase space [15–19], we start with the identification of the magnetic ground state of the Ni sublattice. The extremely ultra thin nature of the samples prohibits the investigation of their magnetic ground state by conventional magnetometry in the background of the large diamagnetic signal from the substrate. To overcome this, we determined the magnetic nature of these superlattices by element resolved XRMS carried out across the Ni $L_{3,2}$ edges with left (I^-) and right (I^+) circularly polarized light. For ultra-thin films, XRMS is a direct spectroscopic probe to elucidate magnetic properties of an electronic shell from a particular atom in multi-component materials [56]. Fig. 2(a) shows the XRMS signal recorded at 25 K in the presence of ± 5 T magnetic field. As seen, the opposite sign of the XRMS signals of the L_3 and L_2 edge at fixed magnetic field (H) along with flipping of the XRMS signal upon reversing the direction of H confirm that the signal is of magnetic origin and intrinsic to the Ni sublattice. In addition, the Ni XRMS signal decreases with reduction of the magnetic field and practically vanishes at 0.1 T (see supplemental [51]). This result immediately excludes the presence of any ferromagnetic ordering within these SLs. To provide further insight, the peak value of XRMS intensity around 852.8 eV is plotted as a function of magnetic field (H). As seen in Fig. 2(b), the obtained linear dependence of the XRMS signal on H implies either a paramagnetic (PM) or antiferromagnetic (AFM) spin configuration of the bilayer. To select between them, the XRMS signal was also measured as a function of temperature in an applied magnetic field of 5 T as shown in Fig. 2(c). As seen, a linear fit to the $1/\text{XRMS}$ vs. T -dependence (Fig. 2(d)) yields a finite value of XRMS at 0 K (i.e. $T_{\text{CW}} \approx -14$ K), implying the presence of AFM spin correlations in the ground state.

Next we discuss the orbital structure investigated by the X-ray linear dichroism (XLD) technique. In the past, XLD has been successfully applied for uncovering different types of orbital ordering and the symmetry of a specific orbital state in various transition metal compounds [57–63]. For this, the geometrical arrangement between the sample and X-ray polarization vector, requires careful consideration for detecting the presence of orbital ordering. Specifically, as seen in Fig. 3(a), all the e_g orbitals ($d_{3z^2-r^2}$, $d_{3x^2-r^2}$, $d_{3y^2-r^2}$) are oriented at $\phi = 54.7^\circ$ with respect to the [111] growth axis for a NiO₆ octahedron. Because of this, the XLD signal is expected to be very small even for a FOO (ferro orbital ordered [51]) state with 100% orbital polarization. In order to maximize the XLD signal, the samples were mounted on a copper wedge (Fig. 3(b)), which reorients the Ni-O bonds along vertical polarization, V and in the plane of horizontal polarization, H. To

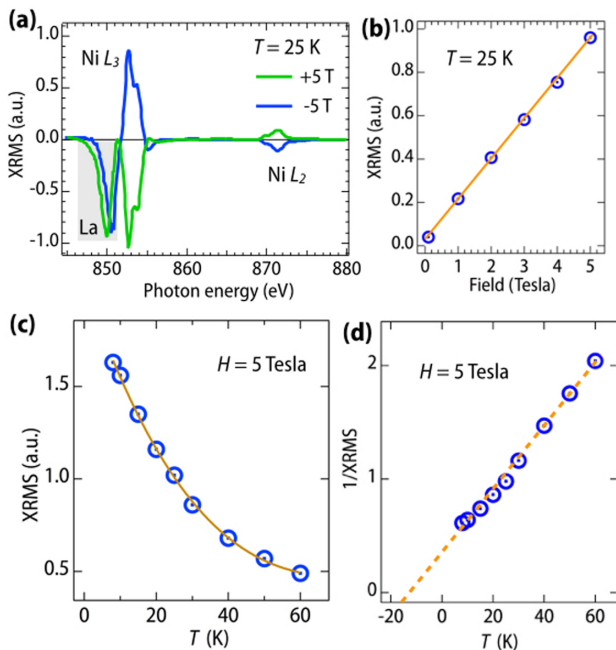


FIG. 2. (a) Ni $L_{3,2}$ -edge XRMS spectra for 2NNO/4LAO sample recorded in an applied magnetic field of ± 5 T. (b) XRMS vs. magnetic field. (c) XRMS vs. T , (d) $1/\text{XRMS}$ vs. T plot. The feature near 850 eV is a contribution from the intense La scattering signal and does not flip with $\pm H$. To eliminate it, the differences (divided by 2) of the XRMS spectra obtained for several positive and negative fields (e.g. ± 5 T) were used for the analysis.

understand how an antiferro orbital ordered state gives rise to a finite XLD signal in this experimental setup, we refer to Fig. 3(c) and 3(d) showing the orientation of $d_{3z^2-r^2}$ and $d_{3x^2-r^2}$ orbitals with respect to the polarization directions H and V for $\theta = 0^\circ$ and 45° respectively. This specific sample orientation with the wedge aligns the $d_{3z^2-r^2}$ orbitals almost along V polarization giving a finite dichroic signal. On the other hand, $d_{3x^2-r^2}$ orbitals are almost aligned in the plane of H polarization with a small but finite angle with respect to the polarization vector H, resulting in an *opposite* and strongly reduced dichroic signal compared to $d_{3z^2-r^2}$ orbitals. As a result, instead of perfect cancellation of linear dichroism, a small finite XLD is expected to be observed for the antiferro orbital ordered (AFO) state analogous to the other well known AFO compounds, e.g. YTiO_3 [57], and $\text{La}_{0.5}\text{Sr}_{1.5}\text{MnO}_4$ [58].

Fig. 3(e) shows resonant Ni L -edge x-ray absorption spectra (XAS) (I_V and I_H) and XLD spectra (difference of I_H and I_V) obtained in the flat ($\theta = 0^\circ$) and wedge ($\theta = 45^\circ$) geometries. As seen, the XAS line shape is in excellent agreement with the expected Ni^{+3} oxidation state akin to the bulk NNO. The multiplet structure in the line shape implies the localized nature of the charge carrier [35, 42] and corroborates the transport results (shown in supplemental [51]). In addition, the observation of the XLD signal for $\theta = 0^\circ$ with a derivative like shape indicates that the Ni e_g orbital degeneracy is indeed lifted in the (111) heterostructure [34]. As an-

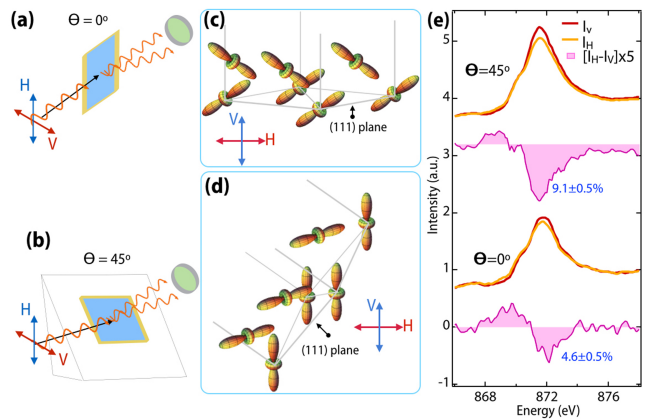


FIG. 3. Experimental arrangement for recording the XLD spectrum for (a) flat ($\theta = 0^\circ$) and (b) wedge ($\theta = 45^\circ$) configuration. θ is the angle between the vertical sample holder and (111) plane of the film. The orbital arrangements for AFO state with the polarization direction for the two experimental configuration have been shown in (c), (d). The Ni XAS recorded (detection mode: total fluorescence yield) at 300 K with V and H polarized light and their differences are shown in (e) for both $\theta = 0^\circ, 45^\circ$. The spectra are shifted vertically for clarity. Note, due to strong overlap of the Ni L_3 -edge with the La M_4 edge, only L_2 edge is shown. Because of the experimental limitation all the measurements were acquired at 45° inclination (instead of ideal 54.7°) relative to the X-ray beam.

anticipated from the discussion above, the XLD signal increased strongly when the measurement was conducted for the $\theta = 45^\circ$ geometry. As expected for the bulk NNO without any orbital ordering [65], our XLD measurements did not find any significant orbital polarization on a thick NNO (111) film (shown in supplemental [51]). This further emphasizes that the observed XLD in 2NNO/4LAO (111) SL is not a measurement artifact and the orbitally polarized ground state is engineered by this buckled honeycomb lattice geometry. The obtained value of XLD around 9% is quite large as the finite bandwidth of the e_g bands and strong covalency [17, 18, 34, 64, 66, 67] reduce the orbital polarization from expected value of atomic limit. We also point out, that this large XLD signal observed in the (111) 2NNO/4LAO system is comparable and even exceeds the values reported for the well established examples of orbitally ordered transition metal compounds [59–63]. It is important to emphasize that by the nature of the spectroscopic probe, XLD can only establish the presence of orbital ordering or orbital polarization but cannot resolve a specific type of the orbital pattern present in the system.

Threefold rotational symmetry is a key element of a buckled honeycomb lattice. To establish the type of orbital pattern responsible for the dichroic effect, we performed density functional theory (DFT) calculations with an on-site Hubbard U term for both ferromagnetic (FM, $\uparrow\uparrow$) and antiferromagnetic (AFM, $\uparrow\downarrow$) spin arrangements of the Ni sites with $P3$ symmetry. The relaxation of internal atomic coordinates retains the trigonal symmetry of the underlying lattice for both FM and AFM cases. For the hypothetical FM spin configura-

tion, the structural relaxation yields two inequivalent Ni layers with magnetic moments of 1.29 and 1.09 μ_B and opens a small gap of 90 meV in the formerly Dirac-point semi-metallic band structure (see Fig. 4(a)). Most importantly, contrary to the experimental observation, the orbital polarization is found to be entirely quenched, as shown in the corresponding spin density plot in Fig. 4(b). The AFM state is found to be less stable compared to the FM state, even though XRMS measurements confirm absence of ferromagnetism. The energetic preference of this FM state, is similar to that obtained for the calculation of bulk nickelates [68, 69], and is attributed to the poor treatment of dynamical screening in ab-initio methods [68]. The issue of the overestimation of ferromagnetic state requires further investigation. The band structure for this AFM solution (shown in Fig. 4(c)) exhibits relatively flat bands with a gap of ~ 0.98 eV. In addition, instead of disproportionating the charge observed in the bulk $RENiO_3$ [69–71], this AFM solution breaks the degeneracy of doubly degenerate e_g levels by a complex *ordered orbital* pattern (spin density shown in Fig. 4(d)). The overall charge distribution (sum over the six sites of a buckled honeycomb lattice) for this pattern is approximately spherical, implying that the expected XLD would be vanishingly small.

Since bulk NNO has orthorhombic (Pbnm) structure and even the ultra thin film of NNO has a strong propensity to retain this symmetry [72], it is crucial to examine the possibility of lowering the symmetry for this 2NNO/4LAO SL grown on rhombohedral LAO. Such symmetry lowering (to monoclinic) had been also reported earlier for the (111) growth of orthorhombic $SrFeO_{2.5}$ (in bulk) on cubic $SrTiO_3$ [25]. Also, we note that while this symmetry breaking is very unlikely in 2 $LaNiO_3$ /4 $LaAlO_3$ (2LNO/4LAO) SL on LAO (111) due to the rhombohedral symmetry of both bulk LNO and LAO, the almost negligible XLD signal for 2LNO/ 4LAO (111) SL (shown in supplemental [51]) strongly suggests the close connection between local symmetry breaking and orbital polarization. In order to elucidate this connection, we have carried out additional DFT+U calculations on a smaller unit cell of 2NNO/4LAO containing 30 atoms (labeled as 1x1 in Fig. 4(e)) with the AFM arrangement of spins. The structural relaxation lowers the symmetry to $P1$ of the lattice. The spin density plotted in Fig. 4(f) for monoclinic AFM structure with equal magnetic moments on each Ni site clearly demonstrates the realization of an antiferro orbital ordering with staggered $d_{3z^2-r^2}$ orbitals rotated by 90° in subsequent layers, i.e. individual (111) planes consisting of $d_{3z^2-r^2}$, $d_{3x^2-r^2}$ orbitals respectively. The band structure shown in Fig. 4(e) also exhibits relatively flat bands with a gap of ~ 1.0 eV with orbital polarization strongly resembling of the artificial double perovskite 1 $LaNiO_3$ /1 $LaAlO_3$ (111) superlattice, where pronounced Jahn-Teller like orbital polarization has been recently reported [19]. Our first-principle calculations thus reveal that natural reduction of the Ni-O hopping interaction from the strong decoupling of triangular Ni layers combined with the breaking of local trigonal symmetry are the decisive factors in the emergence of this orbitally polarized Mott ground state in

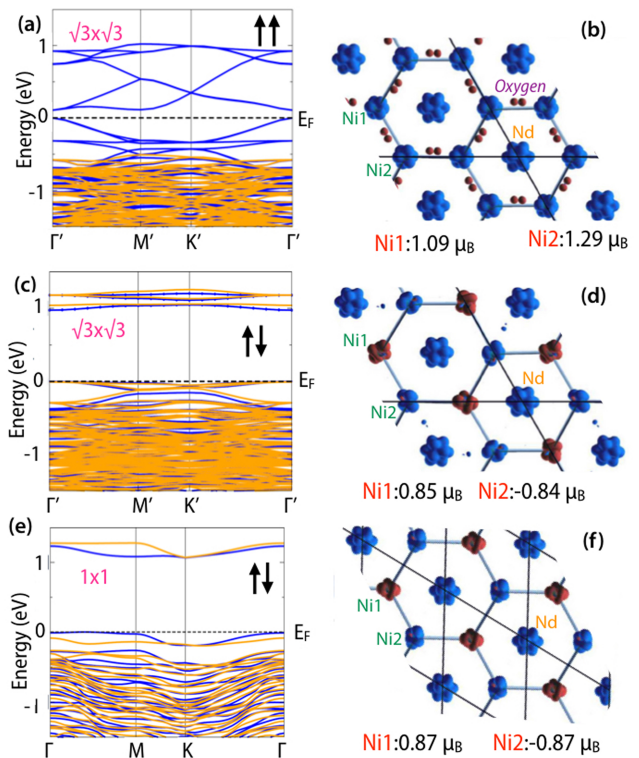


FIG. 4. Majority (blue) and minority (tangerine) band structures for (a) ferromagnetic ($\uparrow\uparrow$) and (c) antiferromagnetic ($\uparrow\downarrow$) order for $(\sqrt{3} \times \sqrt{3})$ supercell. (e) Band structure for ($\uparrow\downarrow$) order on (1×1) supercell. The corresponding spin-density distributions are shown in (b), (d), (f) respectively and also in Supplemental [51].

the bilayer of (111) oriented nickelates.

In summary, by devising bilayers of the rare-earth nickelate $NdNiO_3$ along the pseudo cubic [111] direction, an artificial graphene-like Mott crystal with magnetic d^7 electrons has been realized. The buckled honeycomb lattice with Mott carriers exhibits antiferromagnetic correlations with antiferro orbital order in the ground state, which are unattainable in either bulk $NdNiO_3$ or in analogous heterostructures grown along the conventional (001) direction. These findings open a pathway to exotic Mott and interacting topological states by means of geometrical engineering in buckled honeycomb and dice lattice geometry [13, 14, 21, 73] with many other promising strongly correlated perovskite oxides.

S. M. and J. C. deeply thank D. Khomskii, S. Okamoto, and G. A. Fiete for numerous insightful discussions. S. M. and D. M. were supported by the DOD-ARO under Grant No. 0402-17291. J.C. was supported by the Gordon and Betty Moore Foundations EPiQS Initiative through Grant No. GBMF4534. R. P. and D. D. acknowledge support by the DFG within SFB/TRR80 (project G3). Z. Y., J. S., and L. G. acknowledge National Basic Research Program of China 973 project (2014CB921002, 2012CB921702), Strategic Priority Research Program of the Chinese Academy of Sciences, Grant No. XDB07030200. This research used resources of the Advanced Photon Source, a U.S. Department of Energy

(DOE) Office of Science User Facility operated for the DOE Office of Science by Argonne National Laboratory under Contract No. DE-AC02-06CH11357.

* smiddey@uark.edu

- [1] M. Imada, A. Fujimori, and Y. Tokura, *Rev. Mod. Phys.* **70**, 1039 (1998).
- [2] Y. Tokura, *Rep. Prog. Phys.* **69**, 797 (2006).
- [3] N. P. Armitage, P. Fournier, and R. L. Greene, *Rev. Mod. Phys.* **82**, 2421 (2010).
- [4] D. G. Schlom, L.-Q. Chen, X. Pan, A. Schmehl, and M. A. Zurbuchen, *J. Am. Ceram. Soc.* **91**, 2429 (2008).
- [5] P. Zubko, S. Gariglio, M. Gabay, P. Ghosez, and J.-M. Triscone, *Annu. Rev. Condens. Matter Phys.* **2**, 141 (2011).
- [6] J. Chakhalian, A. J. Millis, and J. Rondinelli, *Nature Mater.* **11**, 92 (2012).
- [7] H. Y. Hwang *et al.*, *Nature Mater.* **11**, 103 (2012).
- [8] J. Chakhalian, *et al. Rev. Mod. Phys.* **86**, 1189 (2014).
- [9] H.-M. Guo, and M. Franz, *Phys. Rev. Lett.* **103**, 206805 (2009).
- [10] H.-M. Guo and M. Franz, *Phys. Rev. B* **80**, 113102 (2009).
- [11] L. Balents, *Nature* **464**, 199 (2010).
- [12] S. R. Giblin, S. T. Bramwell, P. C.W. Holdsworth, D. Prabhakaran and I. Terry, *Nature Phys.* **7**, 252 (2011).
- [13] F. Wang, and Y. Ran, *Phys. Rev. B* **84**, 241103(R) (2011).
- [14] D. Xiao, W. Zhu, Y. Ran, N. Nagaosa, and S. Okamoto, *Nat. Commun.* **2**, 596 (2011).
- [15] K. -Y. Yang, *et al. Phys. Rev. B* **84**, 201104(R) (2011).
- [16] A. Rüegg, and G. A. Fiete, *Phys. Rev. B* **84**, 201103(R) (2011).
- [17] A. Rüegg, *et al. Phys. Rev. B* **85**, 245131 (2012).
- [18] A. Rüegg, *et al. Phys. Rev. B* **88**, 115146 (2013).
- [19] D. Doennig, W. E. Pickett, and R. Pentcheva, *Phys. Rev. B* **89**, 121110(R) (2014).
- [20] X. Hu, A. Rüegg, and G. A. Fiete, *Phys. Rev. B* **86**, 235141 (2012).
- [21] S. Okamoto, *Phys. Rev. Lett.* **110**, 066403 (2013).
- [22] D. Doennig, W. E. Pickett, and R. Pentcheva, *Phys. Rev. Lett.* **111**, 126804 (2013).
- [23] S. Okamoto, *et al. Phys. Rev. B* **89**, 195121 (2014).
- [24] B. Gray, H. N. Lee, J. Liu, J. Chakhalian, and J. W. Freeland, *Appl. Phys. Lett.* **97**, 013105 (2010).
- [25] S. Chakraverty, A. Ohtomo, M. Okude, K. Ueno, and M. Kawasaki, *Crystal Growth & Design* **10**, 1725 (2010).
- [26] M. Gibert, P. Zubko, R. Scherwitzl, J. Iniguez and J.-M. Triscone, *Nat. Mater.* **11**, 195 (2012).
- [27] G. Herranz, F. Sánchez, N. Dix, M. Scigaj, and J. Fontcuberta, *Sci. Rep.* **2**, 758 (2012).
- [28] X. Liu, *et al. Appl. Phys. Lett.* **105**, 042401 (2014).
- [29] X. Liu, *et al. Appl. Phys. Lett.* **106**, 071603 (2015).
- [30] D. Hirai, J. Matsuno, and H. Takagi, *APL Mat.* **3**, 041508 (2015).
- [31] J. L. Blok, X. Wan, G. Koster, D. H. A. Blank, and G. Rijnders, *Appl. Phys. Lett.* **99**, 151917 (2011).
- [32] J. Chaloupka, and G. Khaliullin, *Phys. Rev. Lett.* **100**, 016404 (2008).
- [33] P. Hansmann, *et al. Phys. Rev. Lett.* **103**, 016401 (2009).
- [34] J. W. Freeland, *et al. Europhys. Lett.* **96**, 57004 (2011).
- [35] J. Liu, *et al. Phys. Rev. B* **83**, 161102(R) (2011).
- [36] A. V. Boris, *et al. Science* **332**, 937 (2011).
- [37] E. Benckiser, *et al. Nat. Mater.* **10**, 189 (2011).
- [38] R. Scherwitzl, *et al. Phys. Rev. Lett.* **106**, 246403 (2011).
- [39] J. Chakhalian *et al. Phys. Rev. Lett.* **107**, 116805 (2011).
- [40] M. K. Stewart, J. Liu, M. Kareev, J. Chakhalian, and D. N. Basov, *Phys. Rev. Lett.* **107**, 176401 (2011).
- [41] J. Liu, M. Kargarian, M. Kareev, B. A. Gray, P. Ryan, A. Cruz, N. Tahir, Y.-D. Chuang, J.-H. Guo, J. Rondinelli, J. W. Freeland, G. A. Fiete, and J. Chakhalian, *Nat. Commun.* **4**, 2714 (2013).
- [42] D. Meyers, S. Middey, M. Kareev, M. van Veenendaal, E. J. Moon, B. A. Gray, J. Liu, J. W. Freeland, and J. Chakhalian, *Phys. Rev. B* **88**, 075116 (2013).
- [43] A. Frano, *et al. Phys. Rev. Lett.* **111**, 106804 (2013).
- [44] M. H. Upton, Y. Choi, H. Park, J. Liu, D. Meyers, J. Chakhalian, S. Middey, J.-W. Kim, and P. J. Ryan, *Phys. Rev. Lett.* **115**, 036401 (2015).
- [45] D. Meyers, S. Middey, M. Kareev, J. Liu, J. W. Kim, P. Shafer, P. J. Ryan, and J. Chakhalian, *Phys. Rev. B* **92**, 235126 (2015).
- [46] G. Catalan, *Phase Transitions* **81**, 729 (2008).
- [47] J. L. García-Muñoz, J. Rodríguez-Carvajal and P. Lacorre, *Phys. Rev. B* **50**, 978 (1994).
- [48] X.-L. Qi, and S.-C. Zhang, *Rev. Mod. Phys.* **83**, 1057 (2011).
- [49] S. Middey, *et al. Appl. Phys. Lett.* **101**, 261602 (2012).
- [50] S. Middey, *et al. Sci. Rep.* **4**, 6819 (2014).
- [51] See the Supplementary material.
- [52] K. Schwarz and P. Blaha, *Comp. Mat. Sci.* **28**, 259 (2003).
- [53] P. Blaha, K. Schwarz, G. K. H. Madsen, D. Kvasnicka, and J. Luitz, *WIEN2k, An Augmented Plane Wave Plus Local Orbitals Program for Calculating Crystal Properties*, ISBN 3-9501031-1-2 (Vienna University of Technology, Vienna, Austria, 2001).
- [54] J. P. Perdew, K. Burke, and M. Ernzerhof, *Phys. Rev. Lett.* **77**, 3865 (1996).
- [55] V. I. Anisimov, J. Zaanen, and O. K. Andersen, *Phys. Rev. B* **44**, 943 (1991).
- [56] J. J. Kavich, M. P. Warusawithana, J. W. Freeland, P. Ryan, X. Zhai, R. H. Kodama, and J. N. Eckstein, *Phys. Rev. B* **76**, 014410 (2007).
- [57] F. Iga, *et al. Phys. Rev. Lett.* **93**, 257207 (2004).
- [58] D. J. Huang, *et al. Phys. Rev. Lett.* **92**, 087202 (2004).
- [59] A. Tebano, *et al. Phys. Rev. Lett.* **100**, 137401(2008).
- [60] M. Huijben, *et al. Phys. Rev. B* **78**, 094413 (2008).
- [61] D. Pesquera, *et al. Nat. Commun.* **3**, 1189 (2012).
- [62] N. B. Aetukuri, *et al. Nat. Phys.* **9**, 661-666 (2013).
- [63] Y. K. Kim, *et al. Phys. Rev. Lett.* **111**, 217001 (2013).
- [64] M. Wu, *et al. Phys. Rev. B* **88**, 125124 (2013).
- [65] V. Scagnoli, U. Staub, M. Janousch, A. M. Mulders, M. Shi, G. I. Meijer, S. Rosenkranz, S. B. Wilkins, L. Paolasini, J. Karpinski, S. M. Kazakov, and S. W. Lovesey *Phys. Rev. B* **72**, 155111 (2005).
- [66] M. J. Han, X. Wang, C. A. Marianetti, and A. J. Millis, *Phys. Rev. Lett.* **107**, 206804 (2011); *ibid.* **110**, 179904(E) (2013).
- [67] A. Blanca-Romero, and R. Pentcheva, *Phys. Rev. B* **84**, 195450 (2011).
- [68] G. Gou, I. Grinberg, A. M. Rappe, and J. M. Rondinelli, *Phys. Rev. B* **84**, 144101 (2011).
- [69] H. Park, A. J. Millis, and C. A. Marianetti, *Phys. Rev. Lett.* **109**, 156402 (2012).
- [70] I. I. Mazin, *et al. Phys. Rev. Lett.* **98**, 176406 (2007).
- [71] S. Johnston, A. Mukherjee, I. Elfimov, M. Berciu, and G. A. Sawatzky, *Phys. Rev. Lett.* **112**, 106404 (2014).
- [72] I. C. Tung, *et al. Phys. Rev. B* **88**, 205112 (2013).
- [73] B. Ye, A. Mesaros, and Y. Ran, *Phys. Rev. B* **89**, 201111(R) (2014).